









Numerical investigation of gas-filled multipass cells in the enhanced dispersion regime for clean spectral broadening and pulse compression

V. W. SEGUNDO STAELS,^{1,*}  E. CONEJERO JARQUE,¹  D. CARLSON,²  M. HEMMER,²  H. C. KAPTEYN,²  M. M. MURNANE,² AND J. SAN ROMAN¹ 

¹*Grupo de Investigación en Aplicaciones del Láser y Fotónica, Departamento de Física Aplicada, Universidad de Salamanca, E- 37008, Salamanca, Spain*

²*Department of Physics, JILA and STROBE NSF Science & Technology Center, University of Colorado and NIST, Boulder, Colorado, USA*

*vwsstaels@usal.es

Abstract: We show via numerical simulations that the regime of enhanced frequency chirp can be achieved in gas-filled multipass cells. Our results demonstrate that there exists a region of pulse and cell parameters for which a broad and flat spectrum with a smooth parabolic-like phase can be generated. This spectrum is compatible with clean ultrashort pulses, whose secondary structures are always below the 0.5% of its peak intensity such that the energy ratio (the energy contained within the main peak of the pulse) is above 98%. This regime makes multipass cell post-compression one of the most versatile schemes to sculpt a clean intense ultrashort optical pulse.

© 2023 Optica Publishing Group under the terms of the [Optica Open Access Publishing Agreement](#)

1. Introduction

Self-phase modulation (SPM), the phase shift induced by the optical Kerr effect, is the most widely used spectral broadening nonlinear effect. A few years after the Ruby laser was demonstrated, SPM was identified as one of the possible effects responsible for the spectral broadening observed during nonlinear propagation of laser pulses in various media [1]. In 1978 R. H. Stolen and C. Lin showed a clean experimental demonstration of SPM in an optical fiber [2]. Another relevant milestone in the field of ultrashort pulse generation was reached in 1973, when Hasegawa and Tappert discussed theoretically the possibility of obtaining solitonic laser pulses during their propagation in an optical fiber in the anomalous dispersion regime [3]. These solitons were experimentally demonstrated in 1980 by Mollenauer and coworkers [4]. Almost simultaneously a few experiments, supported by numerical simulations, demonstrated optical pulse compression in an optical fiber in the normal dispersion regime. In these demonstrations, the nonlinear propagation induced a spectral broadening with a spectral phase that had to be compensated with a grating-based compressor [5–7]. Most of these cases were operated in the enhanced frequency chirp regime, in which the nonlinearity dominates the dynamics but the dispersion still plays a non-negligible role and, therefore, pulses without the pronounced spectral modulations related to the SPM are generated [8]. All these milestones constitute the foundations of the different post-compression schemes that have been proposed until today [9].

An important evolution of the post-compression schemes developed in optical fibers in the 1980s was motivated by the appearance of chirped pulse amplification (CPA) laser systems [10], which permitted to noticeably increase the laser peak intensity. The ultra-intense laser pulses delivered by these systems could not be compressed in optical fibers due to both material damage and the appearance of undesirable nonlinear effects. In 1996 however, Nisoli et al.

demonstrated that gas-filled hollow core fibers could be used for nonlinear post-compression of the high intensity optical pulses generated by CPA systems. This post-compression scheme is now ubiquitous in laboratories worldwide but becomes increasingly cumbersome for optical pulses with energies above 1-2 mJ [11].

Alternative post-compression schemes, such as those using thin plates, have been proposed for high-energy Ti:Sapphire [12] and Ytterbium-based laser systems [13,14]. While this multi-plate approach addresses some of the challenges of the HCF-based compressors, it is often cumbersome as it relies on precise placement of the plates – the placement of which is coupled to day-to-day variations in laser parameters –, provides limited control of spatial intensity profile and is ultimately limited in energy handling.

New laser sources, such as the Yb-based laser systems, are gaining interest in both scientific and industrial settings owing to their high average power and repetition rate. Yb-based lasers, that typically feature limited bandwidth (~ 10 nm) yet can operate at orders of magnitude higher average power than Ti:Sapphire systems [13], have motivated the appearance of a different post-compression scheme based on SPM in multipass cells (MPC) [15]. Multipass cell schemes are able to achieve high-average power ultrashort pulses with a homogeneous spatial distribution and a high energy throughput ($>90\%$). These schemes have been demonstrated using either bulk dielectric media [15–19] or gas [19–26] as nonlinear medium inside the MPC. Under some configurations self-compression has been achieved both in gas-filled [27] (theoretically) and in bulk MPCs [28,29], even in the mid-infrared [30]. Moreover, different spatial modes of the cavity have also been used to improve the energy throughput in a gas-filled MPC [31]. For more information related with the state-of-the-art studies on pulse compression in MPCs the reader can refer to two recent reviews [32,33].

In this work, we numerically investigate a regime of nonlinear compression that yields broadband spectra with a smooth spectral phase that is compatible with ultrashort optical pulses with temporal intensity profiles showing negligible side structure. The regime we investigate is akin to that developed in the 80s in optical fiber and relies on enhancing the frequency chirp of the pulses injected into the MPC [8]. It allows temporal compression by an order of magnitude while providing remarkably clean pulses, with 98% of their energy within the main peak of the pulse, with limited spatio-spectral coupling and scalability to high average powers.

2. Numerical model

The 3D numerical model that we have used to simulate the propagation of a laser pulse in the gas-filled MPC is similar to the one presented in [34]. We focus on the spatio-temporal evolution of the envelope of the field affected by diffraction, dispersion, SPM and self-steepening. We neglect the Raman effect, as the propagation takes place in an atomic gas, and the ionization, as the maximum intensity is kept below a relevant ionization threshold. Dispersion in the mirrors is also neglected as it is very small compared to the dispersion introduced during propagation if low-dispersion commercial mirrors are used (see, for example, Ultrafast-Enhanced Silver Concave Laser Mirrors #4017 from Edmund Optics [35]). We solve the nonlinear propagation of the envelope of the field with the standard Split-Step Fourier Method. Therefore, we first solve the linear terms (diffraction and dispersion) both in the Fourier domain in the following way. From the spatio-temporal structure of the envelope of the pulse at a certain position inside the MPC, $A(x, y, z, t)$, we calculate an intermediate envelope structure at $z + \Delta z$ as:

$$\tilde{A}'(k_x, k_y, z + \Delta z, \omega) = \tilde{A}(k_x, k_y, z, \omega) \times \exp\left(ik(\omega)\Delta z\sqrt{1 - \frac{(k_x^2 + k_y^2)}{k^2(\omega)}}\right), \quad (1)$$

where $\tilde{A}(k_x, k_y, z, \omega)$ represents the Fourier transform of $A(x, y, z, t)$ in the two transverse and temporal coordinates, k_x and k_y represent the components of the wavevector in the transverse

coordinates, Δz represents the step in the propagation direction, $k(\omega) = n(\omega)\omega/c$ is the wave vector in the MPC, c is the speed of light in vacuum and $n(\omega)$ is the refractive index of the gas filling the MPC, whose Sellmeier equation for 1 bar is taken from [36]. The refractive index is scaled with pressure as $n^2 - 1 \propto P$. The second step is done in the space and time domain and consists of applying to the intermediate envelope $A'(x, y, z + \Delta z, t) \equiv A'$ the nonlinear terms:

$$A(x, y, z + \Delta z, t) = A' \times \exp \left(i2c\varepsilon_0 k_0 n_2 \Delta z \left[|A'|^2 + \frac{i}{\omega_0} \left(2 \frac{\partial A'}{\partial t} (A')^* + \frac{\partial (A')^*}{\partial t} A' \right) \right] \right), \quad (2)$$

where $k_0 = \omega_0/c$ is the wave vector in vacuum at the central frequency ω_0 , n_2 is the nonlinear refractive index of the gas filling the MPC and $2c\varepsilon_0$ are the constants needed to calculate the optical intensity from the envelope amplitude ($I = 2c\varepsilon_0 |A|^2$), ε_0 being the dielectric permittivity of vacuum. The first term of the nonlinear phase represents the SPM while the second one, that has temporal derivatives, corresponds to the self-steepening. We should note that we work in the retarded frame (a frame moving with the group velocity) [37]. The spatial and temporal windows have been selected so that the beam fits during the whole propagation. The simulations have been done in a grid with 128×128 points in the transverse coordinates and 512 time steps.

3. Results and discussion

3.1. Optimum parameters for broadband pulse generation in gas-filled multipass cells

To achieve a broadband spectra in a gas-filled MPC, compatible with a clean ultrashort pulse, we propose to enter in the enhanced frequency chirp regime and look for the optimal region [8]. In terms of the standard lengths that define the nonlinear propagation dynamics, our optimum regime requires that $L_{NL} < L < L_D$, where L is the total propagation length, and L_{NL} and L_D are the nonlinear and dispersion lengths, respectively, defined as $L_{NL} = 2/k_0 n_2 I_0$ and $L_D = t_0^2/3.11|\beta_2|$ [37]. In these formulae, β_2 is the group velocity dispersion, and I_0 and t_0 represent the peak intensity and the temporal duration at the full width at half maximum (FWHM) of the input pulse, respectively. We also establish an upper limit to the soliton order to assure being in a moderate nonlinear regime. We have chosen $N = \sqrt{L_D/L_{NL}} < 10$ as a reference value. Finally, in order to avoid self-focusing, we impose that the maximum peak power reached during the propagation must be below the critical value, $P_{cr} = 1.8962(\lambda_0^2/4\pi n_0 n_2)$, λ_0 being the central wavelength of the pulse and n_0 the refractive index of the gas at that wavelength [38]. All these conditions define the region of parameters in which we must search in order to generate pulses with the desired features. Besides, and similarly to what has been already proposed in [34], the regime should be in a region in which the ionization and the optical damage in the mirrors of the cell are avoided.

To limit the search to a few parameters, we focus on pulses from standard Ytterbium-based systems, emitting pulses centered at 1030 nm with initial pulse duration of $t_p = 150$ fs. We assume that our initial pulse has a Gaussian temporal profile, $I(t) = I_0 \exp(-2t^2/t_p^2)$. Moreover, we choose a 40 cm long gas-filled confocal multipass cell, formed by two identical mirrors with 40 cm radius of curvature. We consider that the input beam is mode-matched to the cavity.

If we assume that our pulse completes 20 round trips in this multipass cell, so that the total propagation length is 16 meters, the two free parameters that we have to search for the desired pulses are the pulse energy (E) and the gas pressure (p). Figure 1 identifies the $\{E-p\}$ -region for which all the conditions mentioned above are fulfilled, i.e., where we expect to enter the enhanced frequency chirp regime. The region of interest (lighter color in Fig. 1) corresponds to parameters for which the nonlinear interaction is always in a moderate regime and, in our particular situation, is limited to pulse energies below $160 \mu\text{J}$ ($N < 10$), gas pressures below 42 bar ($L < L_D$) and two hyperbolae: $E \cdot p > 60 \text{ bar} \cdot \mu\text{J}$ ($L_{NL} < L$) and $E \cdot p < 1800 \text{ bar} \cdot \mu\text{J}$ ($P_{in} < P_{cr}$).

Note that the optimum $\{E-p\}$ -region is limited by hyperbolae that correspond to constant B-integral values. This is a general trend observed in different nonlinear propagation contexts

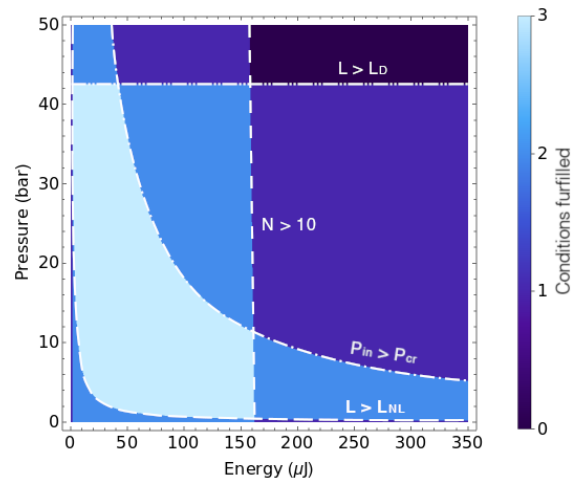


Fig. 1. Region of parameters where the three conditions which limit the enhanced frequency chirp regime are fulfilled. The three conditions are: (I) $L_{NL} < L < L_D$, (II) $1 < N < 10$ and (III) the self-focusing must be avoided ($P_{in} < P_{cr}$). All the parameters are calculated for an Ytterbium-based laser, emitting pulses with a Gaussian temporal profile with initial pulse duration of 150 fs half width at $1/e^2$ centered at 1030 nm, coupled into the fundamental mode of an argon-filled confocal MPC with two identical mirrors of 40 cm radius of curvature, in which the pulse completes 20 round trips. The color code is such that the lighter the color, the more conditions are fulfilled.

[39,40]. It is then clear that we need a B-integral high enough to broaden the spectrum but restricting ourselves to a moderate nonlinear regime. We found the optimum region for our particular situation limited by B-integral values in between 3 and 45 rad, which are relatively moderate B-integral values in the context of MPCs [41]. Once we have identified the $\{E-p\}$ -region that is potentially interesting, we have to determine if the output pulses in this region achieve the clean spectral broadening that we desire. We will do this by performing numerical simulations of the propagation in the particular MPC that we have described before, varying the pulse energy and the gas pressure.

To identify if the output pulse has the desired properties we characterize its spectrum at the end of the propagation with two parameters: first we calculate the spectral width ($\Delta\omega$) as the FWHM of the output spectrum. This width is calculated from $\int \int |\tilde{A}(k_x, k_y, z_{end}, \omega)|^2 dk_x dk_y$, i.e., integrating the intensity profile on the transverse coordinates. The second parameter is the cleanness of the spatially-integrated spectrum, defined as $C = 1 - V$, where $V = (I_M - I_m)/(I_M + I_m)$ is the visibility of the spectral fringes, I_M being the peak value of the spectral intensity and I_m the lowest value of the local minima inside the spectral width $\Delta\omega$. Standard SPM spectra present several spectral maxima, with the higher peaks at the extremes of the spectrum. We identify the highest spectral value and then look for the lowest minima located in between the two spectral high-peaks. If these two values are close, the spectrum is very flat, $V \sim 0$ and $C \sim 1$. By contrast, if the spectrum is strongly modulated, then V approaches 1 and the cleanness is almost 0. If the spectrum does not present a structured shape with local minima, for example if it has a Gaussian-like or similar profile, we identify it as a perfect flat spectrum ($C = 1$), as its corresponding transform limited temporal distribution would present a clean profile with low secondary structures.

Figure 2(a) shows the cleanness (C) of the output spectra when scanning simultaneously pulse energy and gas pressure. We have added contour lines corresponding to those cases where the spectral width ($\Delta\lambda$) is 60 nm, 90 nm and 120 nm. To better see the cleanness obtained in the

optimal region, Fig. 2(b) shows a zoom of the $\{E-p\}$ map with a different color scale. We have not done simulations in the white region as it corresponds to values for which $P_{in} > P_{cr}$, where the nonlinear propagation is so intense that it affects strongly both the spectral and spatial beam structure, entering in the undesired self-focusing region. We assume the 0 bar and 0 μJ cases as linear and assign the same spectral width as the input one and a perfect cleanness value. As it can be seen in Fig. 2(b), the region where short and clean pulses are obtained is part of the optimum region shown in Fig. 1. It is true that Fig. 2(a) indicates that one could use input pulse energies larger than 200 μJ to obtain even broader spectra, but the cleanness (C) deteriorates notably. Moreover, as we use higher pulse energies, we enter in a high solitonic order regime ($N > 10$) where nonlinear terms prevail over linear dispersion, destroying the smoothness of the pulses. We have therefore discarded that high energy region. Regarding the cleanness, we have verified that the sidelobes of the intensity distribution of the transform limited pulse of a case with a $C \geq 0.9$ do not exceed 0.5% of the peak intensity. These are the type of pulses that we want to obtain, hence we propose to work in the energy region around that cleanness value. From the above considerations, we conclude that a good trade off can be found in the region of energies between 50 and 100 μJ and pressures between 10 bar and those defined by the critical power curve. The spectra of the output pulses obtained in this central region is broad enough to generate pulses with transform limit duration in the 15-25 fs range and energy ratio, defined as the fraction of energy contained in the main peak of the pulse, above 98%. Note that a good energy ratio obtained in a standard propagation is around 80% which is a clear indication of the excellent quality of the pulses obtained in our case [26].

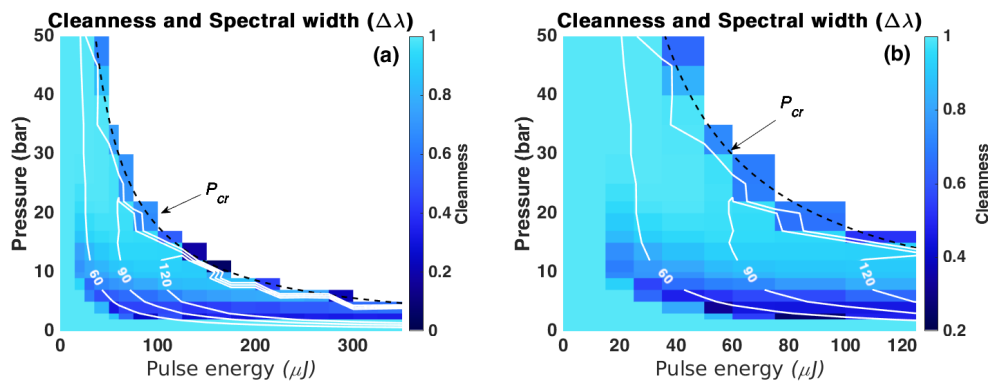


Fig. 2. Pulse cleanness in the energy-pressure map including contour lines for the spectral full width at half maximum ($\Delta\lambda$) shown in nm (a). Zoom of the high cleanness region (b). The dashed line shows the gas pressure at which the critical power (P_{cr}) is reached for each input pulse energy.

3.2. Pulse features under optimal conditions

To illustrate the complete structure of the output pulse that we find under optimum conditions, we analyze here the particular case of an input pulse with 100 μJ of energy in a MPC filled with 10 bar of argon. This particular case is used as an example, yet we have confirmed that similar spectro-temporal features are observed in the vicinity of these $\{E-p\}$ parameters shown in Fig. 2 where the cleanness is close to $C = 0.9$. Figure 3 shows the spatio-spectral distribution integrated in the y axis (Fig. 3(a)) and in the x axis (Fig. 3(b)), and the on-axis temporal (Fig. 3(c)) and spectral (Fig. 3(d)) intensity profiles, including their respective phases. Figure 3(a) and 3(b) confirm that we obtain an excellent spatio-spectral homogeneity, as expected from an MPC [16]. The output pulse (Fig. 3(c)) has a stretched top-hat-like temporal profile on axis due to the

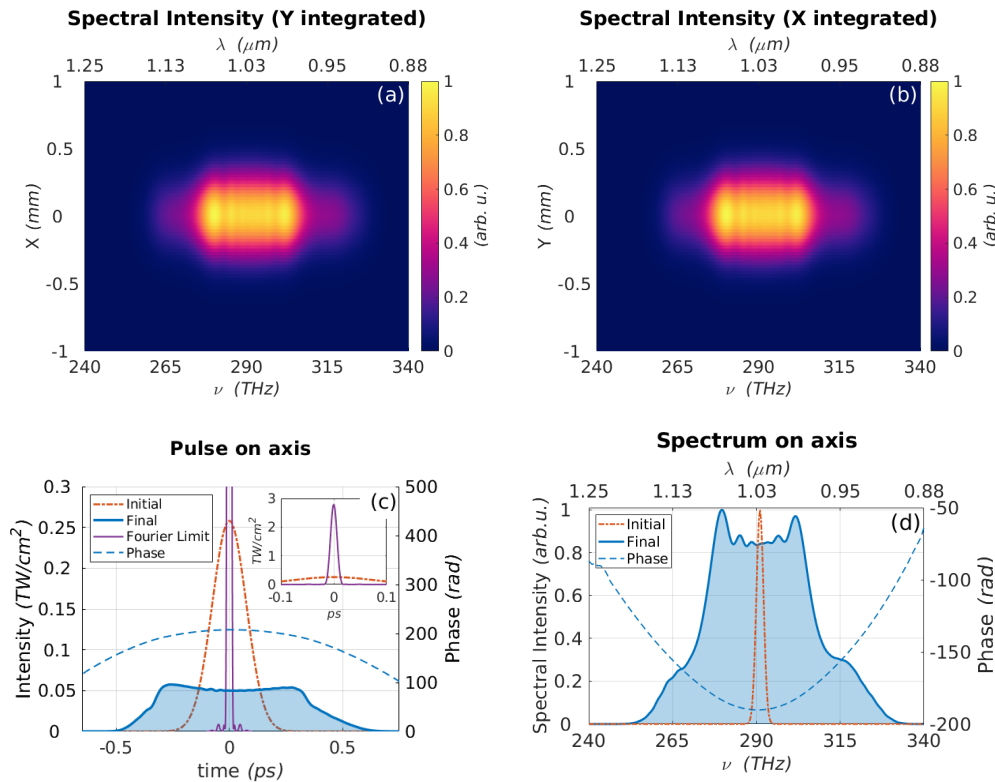


Fig. 3. Results of a simulation in the optimal region which corresponds to a pulse with $100 \mu\text{J}$ of energy in a MPC filled with 10 bar of argon. We show the normalized spatio-spectral distribution integrated in the x axis (a) and y axis (b), and the temporal (c) and (d) spectral on-axis intensity profiles, including their respective phases.

addition of the linear and nonlinear dispersion acquired during the propagation, as expected in the enhanced frequency chirp regime. In fact, the stretching induced during the propagation of the pulse is an essential ingredient to achieve the desired output pulses. This pulse stretching is also responsible to mitigate the contribution of self-steepening during the nonlinear propagation. The inset in this plot shows the temporal profile of the corresponding transform limited pulse which is 14.2 fs long (FWHM), which corresponds to a compression factor of more than 12, and presents an extraordinarily clean profile with a secondary structure below 0.4% of the peak intensity. In fact, the only way to observe the secondary structure of the transform limited pulse is cutting off the upper part, as done in Fig. 3(c), where we show the transform limited pulse together with the input and output pulses. The output on-axis spectrum (Fig. 3(d)) is, as desired, broad (it has a FWHM of 33.2 THz, which corresponds to 118.2 nm) and is also clean with a cleanliness factor $C = 0.91$. The on-axis spectral phase, shown in Fig. 3(d), is smooth along the whole spectrum and, as obtained in past studies in the context of pulse compression in optical fibers [8], it has a dominant positive group delay dispersion that has to be compensated in the compression stage, together with the spectral phase added at the output window of the MPC. Nevertheless, the presence of phase at the input pulse or at the mirrors of the cell might deteriorate the results if their values are large enough.

To have an insight on how the pulse shown in Fig. 3 builds up, Fig. 4(a) shows the evolution of the spectral broadening after each round trip (the FWHM with blue circles and the full width at $1/e^2$ with orange circles) (left y-axis), and the evolution of the cleanliness in purple circles

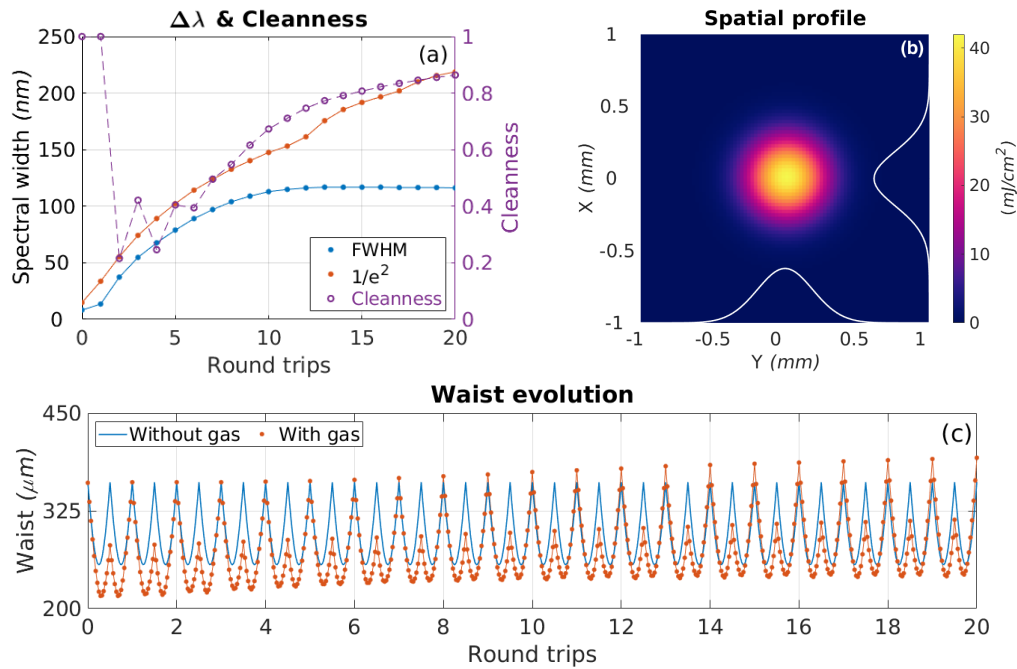


Fig. 4. Panel (a) shows the evolution of the spectral broadening after each round trip (the FWHM with blue circles and the full width at $1/e^2$ with orange circles (left y-axis), and the evolution of the cleanness in purple circles (right y-axis). Panel (b) shows the spatial mode at the end of the propagation. Panel (c) shows the comparison between the linear (blue line) and nonlinear (dots) transverse beam size during the propagation.

(right y-axis). The evolution of the two spectral widths clearly indicate that although the main spectral broadening is done during the first round trips (the first 10 round trips in this case, after which the FWHM stops growing), the evolution of the full width at $1/e^2$ confirms that the tails of the spectrum keep broadening during the whole propagation. In fact, the presence of these spectral tails confirms that we are in the enhanced frequency chirp regime [8]. The evolution of the cleanness (purple circles) is similar to the spectral width at $1/e^2$ as it increases during the entire propagation. The only obvious difference is at the beginning of the propagation, where the spectrum is close to the initial one, i.e. it is non-modulated, and therefore shows a high cleanness. For completeness, Fig. 4(b) shows the spatial mode (the time-integrated spatial intensity distribution) obtained at the end of the propagation, displaying a smooth, symmetrical Gaussian-like profile. In Fig. 4(c) we show the evolution of the beam size (in dots), defined as the radius at which the time-integrated spatial intensity decreases to $1/e^2$ of its peak value. As the spatial distribution keeps the cylindrical symmetry during the whole propagation, we have only plotted the beam size on the x-axis, being identical to the beam size on the y-axis. The first thing to note is the smooth evolution of the beam spatial properties, confirming that the propagation is done in a moderate nonlinear regime that avoids the appearance of any catastrophic spatial dynamics. We have checked that when adding a 5% white noise into the spatial intensity distribution of the beam, the propagation maintains the same spatio-temporal characteristics. We further note that the spatial-mode of the propagation does not correspond to the fundamental spatial-mode of the cell, whose evolution is shown in the blue line in Fig. 4(c). This means that the spatial mode of the beam corresponds to a nonlinear stationary mode of the MPC, as discussed in [41].

The description of the pulses obtained in the optimum $\{E-p\}$ -region is similar to what we have presented in Figs. 3 and 4 for a pulse with 100 μJ of energy in a cell filled with 10 bar of argon. As we have mentioned earlier, we observe that while maintaining the cavity properties and gas pressure, the higher the pulse energy, the larger the spectrum and the lower the cleanliness. Therefore, we confirm that we have been able to generate large and clean spectra with smooth spectral phases in a MPC filled with argon, which paves the way for the generation of few-cycle pulses with a very clean temporal intensity profile.

4. Conclusion

We have shown that pulses with large and clean spectra, compatible with ultrashort and very clean temporal profiles, can be achieved in a multipass cell filled with argon pumped by Ytterbium-based laser systems. We have demonstrated that there is a region in the pulse energy and gas pressure space where these desired pulses are optimally obtained. The final spectrum is achieved thanks to the simultaneous effect of the self-phase modulation and the linear dispersion in the enhanced frequency chirp regime. We have verified that the propagation is done in a stable nonlinear spatial mode of the cell. We believe that these results pave the way for the generation of few-cycle and very clean pulses in the near- and mid-infrared regions.

Funding. Basic Energy Sciences (DE-FG02-99ER14982); Ministerio de Ciencia e Innovación (PRE2020-092181); Ministerio de Ciencia e Innovación (PID2019-106910GB-I00).

Acknowledgments. This work was supported by: PID2019-106910GB-I00 and PRE2020-092181, funded by the Spanish Ministry of Science and Innovation. The US authors gratefully acknowledge support from a DOE Basic Energy Sciences Grant DE-FG02-99ER14982

Disclosures. The authors declare no conflicts of interest.

Data availability. Data underlying the results presented in this paper are not publicly available at this time but may be obtained from the authors upon reasonable request.

Supplemental document. See [Supplement 1](#) for supporting content.

References

1. F. Shimizu, "Frequency broadening in liquids by a short light pulse," *Phys. Rev. Lett.* **19**(19), 1097–1100 (1967).
2. R. H. Stolen and C. Lin, "Self-phase-modulation in silica optical fibers," *Phys. Rev. A* **17**(4), 1448–1453 (1978).
3. A. Hasegawa and F. Tappert, "Transmission of stationary nonlinear optical pulses in dispersive dielectric fibers. I. anomalous dispersion," *Appl. Phys. Lett.* **23**(3), 142–144 (1973).
4. L. F. Mollenauer, R. H. Stolen, and J. P. Gordon, "Experimental observation of picosecond pulse narrowing and solitons in optical fibers," *Phys. Rev. Lett.* **45**(13), 1095–1098 (1980).
5. H. Nakatsuka, D. Grischkowsky, and A. C. Balant, "Nonlinear picosecond-pulse propagation through optical fibers with positive group velocity dispersion," *Phys. Rev. Lett.* **47**(13), 910–913 (1981).
6. C. V. Shank, R. L. Fork, R. Yen, R. H. Stolen, and W. J. Tomlinson, "Compression of femtosecond optical pulses," *Appl. Phys. Lett.* **40**(9), 761–763 (1982).
7. D. Grischkowsky and A. C. Balant, "Optical pulse compression based on enhanced frequency chirping," *Appl. Phys. Lett.* **41**(1), 1–3 (1982).
8. W. J. Tomlinson, R. H. Stolen, and C. V. Shank, "Compression of optical pulses chirped by self-phase modulation in fibers," *J. Opt. Soc. Am. B* **1**(2), 139–149 (1984).
9. T. Nagy, P. Simon, and L. Veisz, "High-energy few-cycle pulses: post-compression techniques," *Adv. Phys.: X* **6**, 1845795 (2021).
10. D. Strickland and G. Mourou, "Compression of amplified chirped optical pulses," *Opt. Commun.* **55**(6), 447–449 (1985).
11. M. Nisoli, S. De Silvestri, and O. Svelto, "Generation of high energy 10 fs pulses by a new pulse compression technique," *Appl. Phys. Lett.* **68**(20), 2793–2795 (1996).
12. C. Lu, Y. Tsou, H. Chen, B. Chen, Y. Cheng, S. Yang, M. Chen, C. Hsu, and A. H. Kung, "Generation of intense supercontinuum in condensed media," *Optica* **1**(6), 400–406 (2014).
13. J. E. Beetar, S. Gholam-Mirzaei, and M. Chini, "Spectral broadening and pulse compression of a 400 μJ , 20 W Yb:KGW laser using a multi-plate medium," *Appl. Phys. Lett.* **112**(5), 051102 (2018).
14. B. Zhu, Z. Fu, Y. Chen, S. Peng, C. Jin, G. Fan, S. Zhang, S. Wang, H. Ru, C. Tian, Y. Wang, H. Kapteyn, M. Murnane, and Z. Tao, "Spatially homogeneous few-cycle compression of yb lasers via all-solid-state free-space soliton management," *Opt. Express* **30**(2), 2918–2932 (2022).

15. J. Schulte, T. Sartorius, J. Weitenberg, A. Vernaleken, and P. Russbueldt, "Nonlinear pulse compression in a multi-pass cell," *Opt. Lett.* **41**(19), 4511–4514 (2016).
16. J. Weitenberg, A. Vernaleken, J. Schulte, A. Ozawa, T. Sartorius, V. Pervak, H.-D. Hoffmann, T. Udem, P. Russbueldt, and T. W. Hänsch, "Multi-pass-cell-based nonlinear pulse compression to 115 fs at 7.5 μ J pulse energy and 300 W average power," *Opt. Express* **25**(17), 20502–20510 (2017).
17. J. Weitenberg, T. Saule, J. Schulte, and P. Rußbüldt, "Nonlinear pulse compression to sub-40 fs at 4.5 μ J pulse energy by multi-pass-cell spectral broadening," *IEEE J. Quantum Electron.* **53**(6), 1–4 (2017).
18. K. Fritsch, M. Poetzlberger, V. Pervak, J. Brons, and O. Pronin, "All-solid-state multipass spectral broadening to sub-20 fs," *Opt. Lett.* **43**(19), 4643–4646 (2018).
19. V. Hariton, A. B. Wahid, G. Figueira, K. Fritsch, and O. Pronin, "Multipass spectral broadening and compression in the green spectral range," *Opt. Lett.* **47**(5), 1246–1249 (2022).
20. M. Ueffing, S. Reiger, M. Kaumanns, V. Pervak, M. Trubetskov, T. Nubbemeyer, and F. Krausz, "Nonlinear pulse compression in a gas-filled multipass cell," *Opt. Lett.* **43**(9), 2070–2073 (2018).
21. L. Lavenu, M. Natile, F. Guichard, Y. Zaouter, X. Delen, M. Hanna, E. Mottay, and P. Georges, "Nonlinear pulse compression based on a gas-filled multipass cell," *Opt. Lett.* **43**(10), 2252–2255 (2018).
22. M. Kaumanns, V. Pervak, D. Kormin, V. Leshchenko, A. Kessel, M. Ueffing, Y. Chen, and T. Nubbemeyer, "Multipass spectral broadening of 18 mJ pulses compressible from 1.3 ps to 41 fs," *Opt. Lett.* **43**(23), 5877–5880 (2018).
23. C. Grebing, M. Müller, J. Buldt, H. Stark, and J. Limpert, "Kilowatt-average-power compression of millijoule pulses in a gas-filled multi-pass cell," *Opt. Lett.* **45**(22), 6250–6253 (2020).
24. Y. Pfaff, C. Forster, G. Barbiero, M. Rampp, S. Klingebiel, J. Brons, C. Y. Teisset, H. Wang, R. Jung, J. Jaksic, A. H. Woldegeorgis, C. J. Saraceno, and T. Metzger, "Nonlinear pulse compression of a thin-disk amplifier and contrast enhancement via nonlinear ellipse rotation," *Opt. Express* **30**(7), 10981–10990 (2022).
25. S. Hädrich, E. Shestae, and M. Tschernajew, *et al.*, "Carrier-envelope phase stable few-cycle laser system delivering more than 100 W, 1 mJ, sub-2-cycle pulses," *Opt. Lett.* **47**(6), 1537–1540 (2022).
26. E. Escoto, A.-L. Viotti, S. Alisaukas, H. Tünnermann, I. Hartl, and C. M. Heyl, "Temporal quality of post-compressed pulses at large compression factors," *J. Opt. Soc. Am. B* **39**(7), 1694–1702 (2022).
27. M. G. Hastings, P. Panagiotopoulos, M. Kolesik, V. Hasson, S. Tochitsky, and J. V. Moloney, "Few-cycle 10 μ m multi-terawatt pulse self-compression in a gas-filled multi-pass cell: a numerical experiment," *J. Opt. Soc. Am. B* **39**(1), 266–272 (2022).
28. G. Jargot, N. Daher, L. Lavenu, X. Delen, N. Forget, M. Hanna, and P. Georges, "Self-compression in a multipass cell," *Opt. Lett.* **43**(22), 5643–5646 (2018).
29. S. Gröbmeyer, K. Fritsch, B. Schneider, M. Poetzlberger, V. Pervak, J. Brons, and O. Pronin, "Self-compression at 1 μ m wavelength in all-bulk multi-pass geometry," *Appl. Phys. B* **126**(10), 159 (2020).
30. D. Carlson, M. Tanksalvala, D. Morrill, J. S. Roman, E. C. Jarque, H. C. Kapteyn, M. M. Murnane, and M. Hemmer, "Nonlinear post-compression in multi-pass cells in the mid-ir region using bulk materials," *Opt. Lett.* **47**(20), 5289–5292 (2022).
31. M. Kaumanns, D. Kormin, T. Nubbemeyer, V. Pervak, and S. Karsch, "Spectral broadening of 112 mJ, 1.3 ps pulses at 5 kHz in a LG10 multipass cell with compressibility to 37 fs," *Opt. Lett.* **46**(5), 929–932 (2021).
32. M. Hanna, F. Guichard, N. Daher, Q. Bournet, X. Délen, and P. Georges, "Nonlinear optics in multipass cells," *Laser Photonics Rev.* **15**(12), 2100220 (2021).
33. A. Viotti, M. Seidel, E. Escoto, S. Rajhans, W. P. Leemans, I. Hartl, and C. M. Heyl, "Multi-pass cells for post-compression of ultrashort laser pulses," *Optica* **9**(2), 197 (2022).
34. M. Hanna, X. Délen, L. Lavenu, F. Guichard, Y. Zaouter, F. Druon, and P. Georges, "Nonlinear temporal compression in multipass cells: theory," *J. Opt. Soc. Am. B* **34**(7), 1340–1347 (2017).
35. Edmund Optics, Ultrafast-Enhanced Silver Concave Laser Mirrors #4017.
36. M. N. Polyanskiy, "Refractive index database," <https://refractiveindex.info>. Accessed on 2022-03-09.
37. G. P. Agrawal, *Nonlinear Fiber Optics* (Academic Press, 2013).
38. G. Fibich and A. L. Gaeta, "Critical power for self-focusing in bulk media and in hollow waveguides," *Opt. Lett.* **25**(5), 335–337 (2000).
39. C. M. Heyl, H. Coudert-Alteirac, M. Miranda, M. Louisy, K. Kovacs, V. Tosa, E. Balogh, K. Varjú, A. L'Huillier, A. Couairon, and C. L. Arnold, "Scale-invariant nonlinear optics in gases," *Optica* **3**(1), 75–81 (2016).
40. M. F. Galán, E. C. Jarque, and J. S. Roman, "Optimization of pulse self-compression in hollow capillary fibers using decreasing pressure gradients," *Opt. Express* **30**(5), 6755–6767 (2022).
41. M. Hanna, L. Daniault, F. Guichard, N. Daher, X. Délen, R. Lopez-Martens, and P. Georges, "Nonlinear beam matching to gas-filled multipass cells," *OSA Continuum* **4**(2), 732 (2021).